Dislocation Mechanics–Based Constitutive Equations

FRANK J. ZERILLI

A review of constitutive models based on the mechanics of dislocation motion is presented, with focus on the models of Zerilli and Armstrong and the critical influence of Armstrong on their development. The models were intended to be as simple as possible while still reproducing the behavior of real metals. The key feature of these models is their basis in the thermal activation theory propounded by Eyring in the 1930's. The motion of dislocations is governed by thermal activation over potential barriers produced by obstacles, which may be the crystal lattice itself or other dislocations or defects. Typically, in bcc metals, the dislocation-lattice interaction is predominant, while in fcc metals, the dislocation-dislocation interaction is the most significant. When the dislocation-lattice interaction is predominant, the yield stress is temperature and strain rate sensitive, with essentially athermal strain hardening. When the dislocation-dislocation interaction is predominant, the yield stress is athermal, with a large temperature and rate sensitive strain hardening. In both cases, a significant part of the athermal stress is accounted for by grain size effects, and, in some materials, by the effects of deformation twinning. In addition, some simple strain hardening models are described, starting from a differential equation describing creation and annihilation of mobile dislocations. Finally, an application of thermal activation theory to polymeric materials is described.

I. INTRODUCTION

IN the 1970s and 1980s, as well as in more recent years, there has been a great deal of interest in constitutive relations that could describe material behavior sufficiently well enough to produce accurate predictions of deformation and fracture when used in large scale computer simulations. An important advance was made by Johnson and Cook,[1] who successfully described cylinder impact (Taylor) test results for a variety of materials using the Lagrangian material-dynamics code EPIC-2, which they had developed. They employed a temperature and strain rate-dependent constitutive relationship relating the von Mises yield stress to the von Mises effective strain:

$$\sigma = (A + B\varepsilon^n)(1 + C \ln \dot{\varepsilon})(1 - T^{*m}) \qquad [1]$$

where $\dot{\varepsilon}$ is the strain rate, T^* is the ratio $(T - T_{\text{room}})/(T_{\text{melt}} - T_{\text{room}})$, and T is the absolute temperature. The terms A, B, n, C, and m are material constants determined from limited straining tests done in tension or torsion. In this equation, strain hardening, strain rate hardening, and thermal softening are taken into account, but it turns out that the variation of thermal softening with strain rate is not reproduced well for real materials.

Since 1934, when Taylor,[2] Orowan,[3] and Polany,[4] trying to understand slip in crystals, independently proposed that the presence of imperfections, in particular, edge dislocations, is able to account for the discrepancy between the large theoretical shear strength and the much lower observed strength of metals, considerable research has been done in developing a dislocation mechanics basis for describing material behavior. The key to this dislocation mechanics description is the description of the motion of dislocations by means of Eyring's thermal activation theory.[5] In the 1960s and 1970s, a number of researchers, including Armstrong, developed these ideas, and most of the recent work has drawn upon this body of knowledge. The mechanical threshold stress model of Follansbee and Kocks[6] incorporates these ideas to describe the temperature, strain rate, and even evolutionary history dependence of the flow stress.

One of the simplest dislocation mechanics formulations was propounded by Armstrong and described in 1987 by Zerilli and Armstrong,[7] in which heuristic arguments, based on the idea of the thermally activated motion of dislocations, were used to derive relations for fcc and bcc metals. Armstrong also pointed out the need for certain athermal effects due to grain size and related deformation twinning, to be treated separately and explicitly.

The nature of the dislocation interactions leads to different forms for the fcc and bcc equations. For bcc metals, the motion of dislocations is governed by the Peierls–Nabarro stress resulting from the interaction produced by the overall lattice potential. This leads to little increase in flow stress ("strain hardening") with strain. For fcc metals, the motion of dislocations is constrained by their mutual intersections, leading to substantial strain hardening. The hcp metals have a stress strain behavior falling somewhere between bcc and fcc metals.

II. THERMAL-ACTIVATION MODEL

In the thermal activation picture, the dislocations are assumed to move in a periodic potential, and the average dislocation velocity is determined by the thermodynamic probability for achieving sufficient energy at temperature T to move past a peak in the potential.

By simple geometry, the glide-plane shear strain rate $\dot{\gamma}$ is related to the average dislocation velocity v by

$$\dot{\gamma} = \rho_m b v \qquad [2]$$

FRANK J. ZERILLI, Senior Scientist, is with the Research and Technology Department, Naval Surface Warfare Center Indian Head Division, Indian Head, MD 20640. Contact e-mail: zerillifj@ih.navy.mil

This article is based on a presentation given in the symposium "Dynamic Deformation: Constitutive Modeling, Grain Size, and Other Effects: In Honor of Prof. Ronald W. Armstrong," March 2–6, 2003, at the 2003 TMS/ASM Annual Meeting, San Diego, California, under the auspices of the TMS/ASM Joint Mechanical Behavior of Materials Committee.

where ρ_m is the areal density of mobile dislocations and b is the magnitude of the dislocation Burgers vector. The average dislocation velocity can then be written in terms of a Gibbs free energy, a function of T and the thermal component of stress τ. The form of the Gibbs function is determined by assuming that the area of activation,

$$A = -\frac{1}{b}\left(\frac{\partial G}{\partial \tau}\right)_T \quad [3]$$

is inversely proportional to the glide plane shear stress.[8]

While much more complicated expressions have been proposed for the dependence of the activation area on shear stress (refer to the monograph of Kocks *et al.*[9]), the inverse-proportionality assumption has given extremely good results for a wide range of materials from metal to polymers. Even in the early 1970s, there was some theoretical and experimental justification for this choice. Hartley,[10] using a simple model for the dislocation intersection mechanism, showed that A was inversely proportional to glide-plane shear stress for small stresses. Similarly, in the case of the Peierls–Nabarro stress due to the dislocation lattice interaction, Feltham[11] showed that A is proportional to $\tau^{-1/2}$ for small stresses and to $\tau^{-3/2}$ for large stresses, with an intermediate range in which A is inversely proportional to τ. Experimentally measured activation areas also showed a close correspondence to the inverse proportionality relation.[12] At a very high shear stress, or, equivalently, low temperatures, A approaches a nonzero constant A_0.

The result is that the thermal component of stress may be written as

$$\sigma_{Th} = Be^{-\beta T} \quad [4]$$

where

$$B \propto \frac{1}{A_0} \quad [5]$$

and

$$\beta = \beta_0 - \beta_1 \ln \dot{\varepsilon} \quad [6]$$

For bcc metals, A_0 is considered to be constant. In fact, it was the observation that A_0 is essentially independent of plastic strain for a number of bcc metals, including reasonably pure iron, molybdenum, and niobium, that led to the interpretation that the intrinsic Peierls stress associated with the movement of an isolated dislocation is responsible for their thermal-activation behavior.[13]

For fcc metals, A_0, determined by dislocation intersections, is proportional to the inverse square root of strain.[7] Therefore, for fcc metals, B may be written as

$$B = B_0\varepsilon^{1/2} \quad [7]$$

To obtain the total flow stress, a constant term describing the influence of solutes and grain boundaries must be added to the thermal stress, so that the complete constitutive relation for fcc metals is

$$\sigma = \sigma_{Th} + \sigma_G + k_H\ell^{-1/2} \quad [8]$$

where σ_G is the contribution due to solutes and initial dislocation density, k_H is the microstructural stress intensity, and ℓ is the average grain diameter. For bcc metals, an additional empirical term of the form $K\varepsilon^n$ is added to describe the strain dependence. In theory, n is 1/2 in this case as well.

In summary, the relation for fcc metals is

$$\sigma = c_0 + B_0\varepsilon^{1/2}e^{-\beta T} \quad [9]$$

and for bcc metals is

$$\sigma = c_0 + Be^{-\beta T} + K\varepsilon^n \quad [10]$$

where

$$c_0 = \sigma_G + k_H\ell^{-1/2} \quad [11]$$

General Constitutive Equation

In order to describe the intermediate behavior of hcp materials and certain alloy steels, we later introduced both Peierls stress type interactions and intersection of forest-dislocations type interactions into a single equation written in the form

$$\sigma = \sigma_a + Be^{-\beta T} + B_0\varepsilon^{1/2}e^{-\alpha T} \quad [12]$$

where

$$\beta = \beta_0 - \beta_1 \ln \dot{\varepsilon} \quad [13]$$

and

$$\alpha = \alpha_0 - \alpha_1 \ln \dot{\varepsilon} \quad [14]$$

As it turns out, this equation gives a very good representation for the constitutive relation for HY-100 steel, which has characteristics of both fcc and bcc metals.[14] The fcc and bcc equations are just special cases of this more general equation.

III. APPLICATIONS

The constitutive relations were applied to the description of several materials, and they were found to describe the major features of the material deformation behavior reasonably well. These features include the flow stress and tensile-instability strain as functions of temperature, strain rate, and grain size. The equations do not describe features such as the upper and lower yield points, related strain-aging phenomena, and deformation twinning, all common in bcc and hcp metals. Of these, deformation twinning is the most important when an accurate prediction of deformation is required.

A. *FCC Metals—Copper*

The first application of the fcc equation was in modeling an OFHC copper Taylor cylinder impact.[7] For this purpose, the equation was incorporated into the EPIC-2 code[1] to describe the relation of the von Mises effective stress to effective strain. The constants for the model were obtained from tensile and torsion test data reported by Johnson and Cook.[1,15] Figure 1 shows the improved accuracy of the thermal-activation model compared with the Johnson–Cook model. The equation also produced good results in predicting deformation behavior under a variety of conditions of temperature, strain rate, and grain size in expanding-ring experiments.[16]

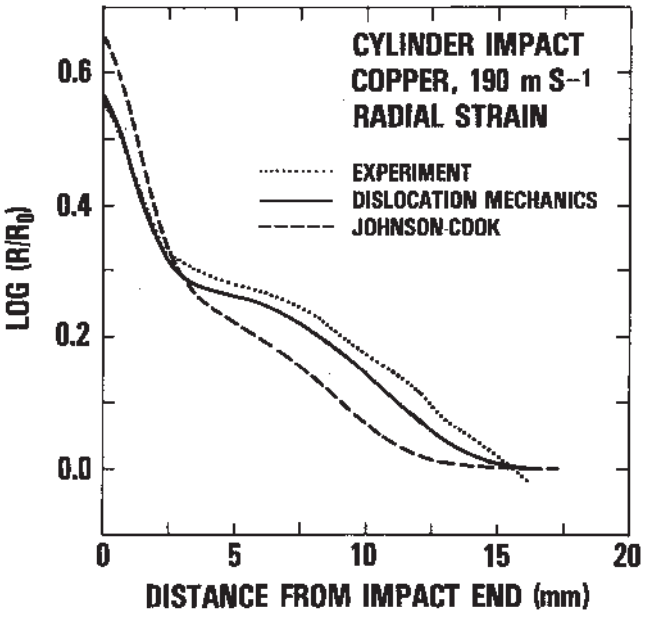

Fig. 1—Radial strain *vs* distance from the impacted end for the 190 m/s copper cylinder impact test. The dotted line is the experimental result of Johnson and Cook, the dashed line is the EPIC-2 simulation result based on the Johnson–Cook constitutive relation, and the solid line is the EPIC-2 simulation result based on the fcc dislocation mechanics thermal activation equation.

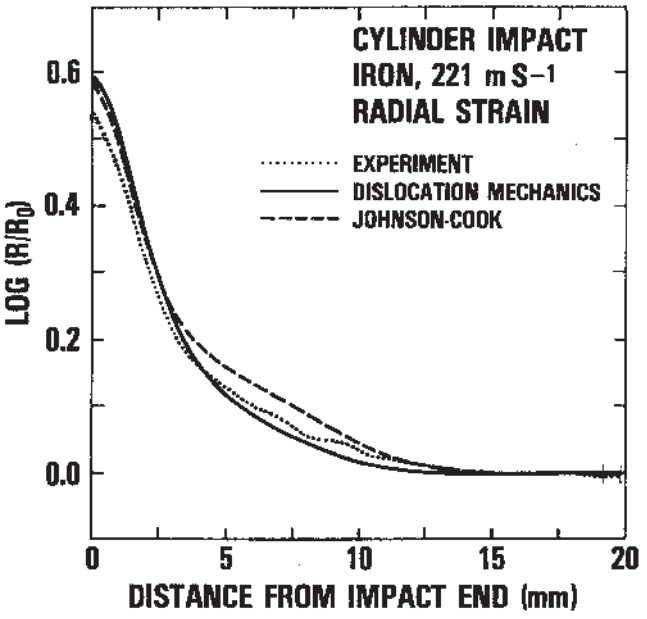

Fig. 2—Radial strain *vs* distance from the impacted end for the 221 m/s iron cylinder impact test. The dotted line is the experimental result of Johnson and Cook, the dashed line is the EPIC-2 simulation result based on the Johnson–Cook constitutive relation, and the solid line is the EPIC-2 simulation result based on the bcc dislocation mechanics thermal activation equation.

B. *BCC Metals—Iron*

In the first application of the bcc equation, an iron Taylor-cylinder impact was modeled.[7] Again, the equation was implemented in the EPIC-2 code, and the constants for the model were obtained from tensile and torsion test data reported by Johnson and Cook. The results are shown in Figure 2. Although the model is reasonably good, it is seen from the deformation of the cylinder at the impact end that the material is harder than predicted by the calculation. The effect is small but unmistakable, and no fudging of the model parameters could reproduce it. This led to the conclusion that deformation twinning in iron was responsible for the additional hardening.

Armstrong noted that deformation twinning is important in certain bcc metals and occurs when a certain threshold stress, depending on grain size and little else, is exceeded. The dependence of the twinning threshold stress on grain size may be written as

$$\sigma_T = \sigma_{T0} + k_T \ell^{-1/2} \qquad [15]$$

which is similar to the dependence of the athermal part of the flow stress on grain size.[7,17] For iron, σ_{T0} is 330 MPa and k_T is 90 MPa-mm$^{1/2}$. The grain size of the cylinder test material was about 100 μm; thus, twinning would occur at a stress level of 600 MPa. This stress will be achieved at the impact end of the cylinder in impacts of 200 ms^{-1}, in which strain rates of 10^4 s^{-1} are generated. Twinning had been shown to occur in fcc metals, but generally at very much higher stress levels. For copper, the stress levels are in the range of 1600 to 2800 MPa.[18] Twinning would harden the material, because twin boundaries could be as effective as grain boundaries in immobilizing dislocations.

The hypothesis that twinning was responsible for the additional hardening was confirmed with a simple addition to the numerical model. From photomicrographs of the impacted specimen, Armstrong determined that, at the impacted end, each grain contained approximately four twins. With this information and the value of 22 MPa-mm$^{1/2}$ for the microstructural stress intensity k_H for iron, it could be inferred that the twinned grains were hardened by about 83 MPa. The twinning would occur above a threshold stress of 600 MPa. So, the numerical model was modified to add 83 MPa to the yield stress in any computational cell in which the flow stress at any time exceeded 600 MPa. The result was the almost perfect agreement between computation and experiment shown in Figure 3.

Tantalum, a bcc metal, shows little susceptibility to twinning, and, so, constants derived from independent data give a good description of its deformation behavior.[19] In our study, a range of values for σ_G was given. The value to be used for a particular material would depend on the solute concentration and could be determined by a yield stress measurement.

Constants for tungsten were obtained from experimental data of Bechtold and Shewmon[20] and Bechtold,[21] which covered strain rates from 10^{-2} to 10^{-5} s^{-1} and temperatures from 450 to 1175 K. Three sets of constants were obtained that could equally well fit these high temperature, low strain-rate data.[22] The constants were applied to predict the ductile-brittle transition behavior.

Flyer plate impact experiments for iron and tantalum have also been successfully described by the bcc equations.[23]

C. *Deformation Twinning*

As we have seen, twinning must be taken into account when modeling the deformation of iron at high strain rates.

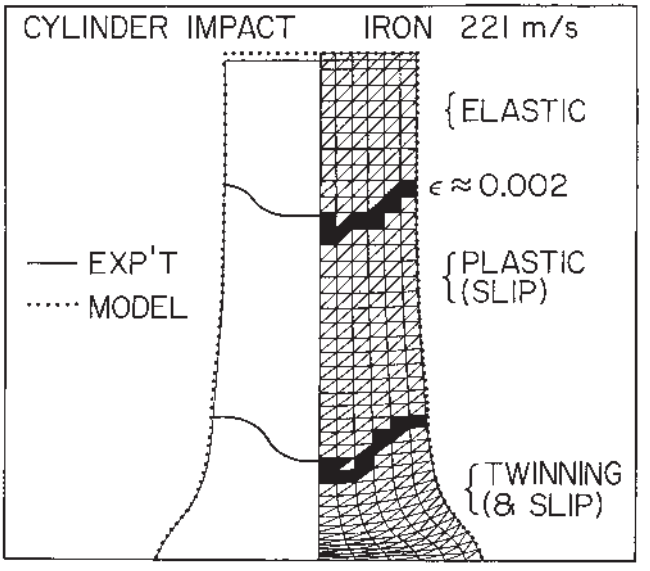

Fig. 3—Confirmation that deformation twinning was responsible for the failure of the bcc constitutive equation to simulate the hardness of the iron cylinder impact specimen at the impact end. Good result when computational cells in which the Mises stress exceeds 600 MPa have their yield stress increase by 83 MPa.

The method that was used to confirm the effect of twinning was based upon the premise that twinning effectively refines the grain size.[24] If a grain reaches the appropriate stress level, it is considered twinned and a constant increment is added to the flow stress. Once twinned, the new threshold stress is much higher than the original one, so further twinning is unlikely to occur. Unfortunately, this model requires *a priori* knowledge of the number of twins per grain. However, this leads to the idea that enough twinning will occur in a grain to accommodate the excess by which the von Mises equivalent stress exceeds the twinning threshold stress. That is, the twinning will be just sufficient to harden the material up to the current local value of the von Mises stress. Under conditions of plastic flow, the von Mises stress is equal to the flow stress, so the implementation of a model based on this idea consists of calculating a new effective grain size by setting $\sigma = \sigma_T$, with the result that[25]

$$\ell = \left(\frac{k_T - k_H}{\sigma_0 - \sigma_{T0}} \right)^2 \qquad [16]$$

where

$$\sigma_0 = \sigma_G + Be^{-\beta T} + K\varepsilon^n \qquad [17]$$

Note that, for Eq. [16] to have a physically meaningful solution, σ_0 must be greater than $\sigma_{\tau 0}$. The locus of points for which $\sigma_0 = \sigma_{\tau 0}$ gives a relation between strain rate, temperature, and strain that determines the conditions under which twinning will occur. So, for example, in iron ($\sigma_G = 0$, $B = 1033$ MPa, $\beta_0 = 6.98 \times 10^{-3}\ \mathrm{K}^{-1}$, $\beta_1 = 4.15 \times 10^{-4}\ \mathrm{K}^{-1}$), at 300 K and zero plastic strain, the strain rate must exceed $2000\ \mathrm{s}^{-1}$ for twinning to occur.

This model was applied to the hcp metals titanium and zirconium, both of which tend to exhibit a behavior similar to bcc metals and both of which twin readily. The base constants were obtained from data published by Ramachandran *et al.*[26] As can be seen from Figures 4 and 5, the effect of twinning is quite striking in the case of titanium.[27]

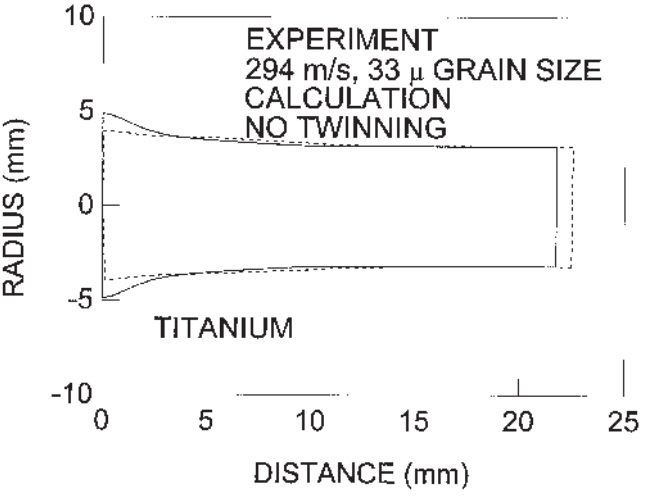

Fig. 4—Titanium cylinder impact, experimental data of Holt *et al.*[27] Simulation fails when twinning not taken into account.

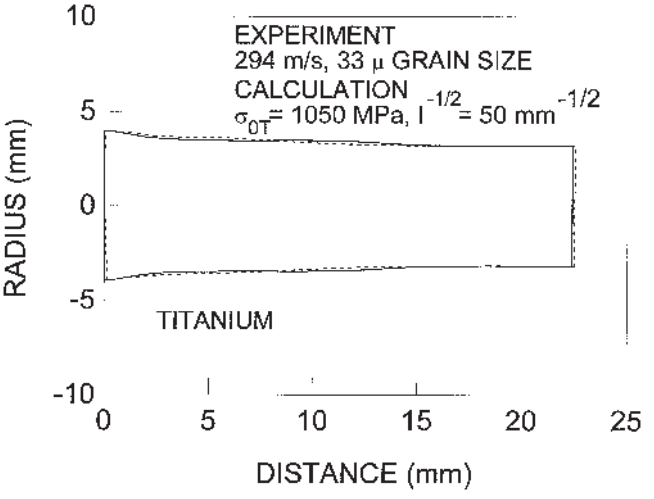

Fig. 5—Titanium cylinder impact, experimental data of Holt *et al.*[27] Good result is achieved with twinning model based on refining effective grain size until twinning threshold stress rises to current value of local Mises stress.

D. *Tensile Instability*

The condition for stability against necking in a tensile test is that the rate of strain hardening of the test material be sufficient to overcome the loss of load-bearing capability due to reduction of cross section. In mathematical terms,

$$\frac{d\sigma}{d\varepsilon} > \sigma \qquad [18]$$

The Eqs. [9] through [11] have successfully described the necking behavior of copper[8,13] and tantalum[18,28] as functions of temperature and strain rate, showing the contrasting behavior of fcc and bcc metals: the uniform strain before necking increases with strain rate for fcc metals and decreases with strain rate for bcc metals. The fcc instability condition was used[8] to discount dislocation drag being responsible for

observations of a significant upturn in flow stress of copper at strain rates greater than 10^3 s^{-1}.

IV. STRAIN HARDENING AND RECOVERY

Up to this point, we have been satisfied with a strain hardening proportional to the square root of plastic strain, a relation originally derived by Taylor.[29] At the same time, Taylor and Quinney,[30] in a pioneering study, observed saturation in the flow stress of copper compressed to a strain of 4. Although the Taylor strain hardening works reasonably well for small strains, the flow stress generally falls below that given by the parabolic law at larger strains. The use of a power law strain hardening with a power of somewhat less than 1/2 is an attempt to account for this approach to saturation. Following work by Bergstrom,[31] Klepaczko,[32] and Estrin and Mecking,[33] it is possible to extend Taylor strain hardening to include dynamic recovery and the consequent saturation of the stress-strain curve at large strains. A similar approach with somewhat different assumptions was undertaken by Follansbee and Kocks in including dynamic recovery in their description of OFE copper.[6]

At low temperatures, in the absence of thermal fluctuations, the flow stress is related to the areal density of dislocations ρ by

$$\hat{\sigma}_{Th} = \hat{\alpha}\mu b\sqrt{\rho} \qquad [19]$$

where $\hat{\alpha}$ is a constant of the order of unity which depends on the geometry and strength of the dislocation-dislocation interaction, μ is the shear modulus, and b is the magnitude of the Burgers vector. This result was originally obtained by Taylor,[2] and a number of strain hardening models lead to this relation, as is discussed in some detail by McClean.[34] In the case of hardening due to dislocation-dislocation interactions, the relation arises because the forces between dislocations are inversely proportional to the distance between them, and the areal density of dislocations is inversely proportional to the square of the distance between them.

Taking a heuristic approach, the density of immobile dislocations may be related to the strain by the differential equation

$$\frac{d\rho_i}{d\varepsilon} = \frac{1}{b\lambda} - \omega\rho_i \qquad [20]$$

where λ is the mean free path for immobilization of mobile dislocations, and ω is the probability for remobilizing or annihilating a stopped dislocation. If $\omega = 0$, then with constant λ, the solution of this evolution equation results in

$$\varepsilon = \rho_i b\lambda \qquad [21]$$

which leads to Taylor strain hardening, $\hat{\sigma} \propto \sqrt{\varepsilon}$. For simplicity, it is assumed that the initial density of immobile dislocations is zero.

How is it that the density of immobile dislocations appears in Eq. [21], when it is the mobile dislocations that produce strain? The answer is that, in this picture, exactly ρ_i mobile dislocations per unit area are created and become immobilized after moving an average distance of λ. The creation of mobile dislocations is described by the equation

$$\frac{d\rho_m}{d\varepsilon} = \frac{c_m - a_m}{\dot{\varepsilon}} - \frac{d\rho_i}{d\varepsilon} \qquad [22]$$

where ρ_m is the density of mobile dislocations, and c_m and a_m are the creation and annihilation rates for mobile dislocations, respectively, the forms of which need not be specified here.

If ω is a nonzero constant, a simple extension to Taylor strain hardening is obtained that exhibits a saturation stress. In this case, the cold flow stress becomes

$$\hat{\sigma} = B_0\sqrt{\varepsilon_r(1 - e^{-\varepsilon/\varepsilon_r})} \qquad [23]$$

where $B_0 = \hat{\alpha}\mu\sqrt{b/\lambda}$, and $\varepsilon_r = 1/\omega$ is a characteristic strain for recovery. At temperatures above zero, this cold flow stress is reduced by the thermal activation factor, and Eq. [12] becomes

$$\sigma = \sigma_a + Be^{-\beta T} + B_0\sqrt{\varepsilon_r(1 - e^{-\varepsilon/\varepsilon_r})}\, e^{-\alpha T} \qquad [24]$$

Figure 6 shows a comparison of Eqs. [12] and [24] using constants derived for tantalum from data of Chen *et al.*[35] A value of ε_r of 1.0 fits their large strain data well.

With a slightly more complicated form for λ,

$$\lambda = \lambda_0 + 1/\sqrt{\rho} \qquad [25]$$

a strain hardening law is obtained which exhibits an initial linear strain hardening and an intermediate Taylor behavior, with an ultimate saturation of the flow stress at large strains. The form is physically reasonable, as it expresses the fact that the mean free path is large (and equal to the average distance between dislocations) for small dislocation densities, but has a lower limiting value for large dislocation densities. With this strain-hardening law, an excellent fit to the stress-strain behavior of pure polycrystalline copper may be obtained.[36]

V. POLYMERS

A. *General Thermal-Activation Model*

We now would like to turn our attention to the general description of the thermal activation model with a view

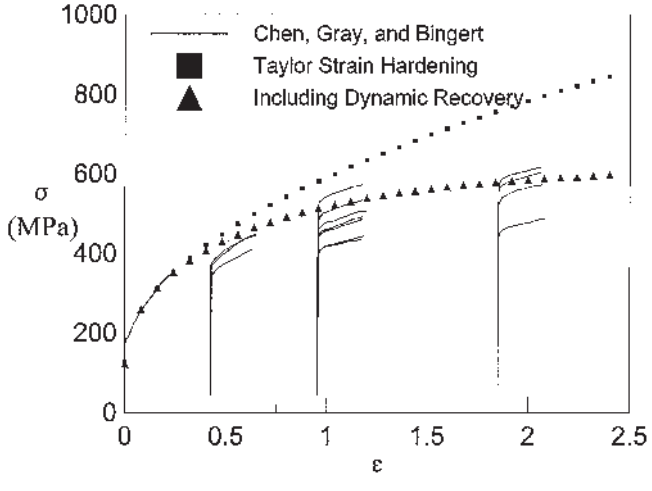

Fig. 6—Computed stress *vs* strain for tantalum at $T = 298$ K, $\dot{\varepsilon} = 10^{-3}$ s^{-1}. The squares depict the best fit ($\sigma a = 130$ MPa, $B_0 = 460$ MPa) Taylor ($\sigma_a + B_0\sqrt{\varepsilon}$) strain hardening to the small strain data of Chen *et al.*[35] The triangles represent the relation $\sigma_a + B_0\sqrt{\varepsilon_r(1 - e^{-\varepsilon/\varepsilon_r})}$ where the recovery strain $\varepsilon_r = 1$ and $\sigma_a = 120$ MPa, $B_0 = 500$ MPa.

toward describing its application to polymers. The thermal-activation model describes the rate of any process in which matter rearranges by surmounting a potential energy barrier. When the potential barrier is sufficiently high, the rate in the forward direction exceeds the reverse rate significantly, and the plastic strain rate is given by the expression[37]

$$\dot{\varepsilon} = \dot{\varepsilon}_0 e^{-G/kT} \quad [26]$$

where G is the activation energy for the reaction, k is Boltzmann's constant, and T is the absolute temperature. The term G may be identified with the Gibbs free energy, so we may write the standard thermodynamic relation

$$dG = -S\,dT - V_{ij}\,d\sigma_{ij} \quad [27]$$

where S is the entropy, and the volumes of activation V_{ij} are the thermodynamic variables conjugate to the stresses σ_{ij}. At constant temperature, specializing to isotropic materials and assuming that there is no dependence on the third stress invariant, Eq. [26] may now be written as

$$\int V_\sigma\,d\sigma = \int V_{kk}\,dp + G_0 + kT\,\ln(\dot{\varepsilon}/\dot{\varepsilon}_0) \quad [28]$$

where we assume that V_σ is a function of effective stress σ and pressure p and that V_{kk} is a function only of pressure.

Assuming that the effective stress-activation volume depends inversely on the effective stress,

$$V_\sigma = \frac{W_0(p)}{\sigma} \quad [29]$$

and solving for the effective stress, Eq. [28] becomes

$$\sigma = B(p)\,e^{-\beta(p,\dot{\varepsilon})T} \quad [30]$$

where the function $B(p)$ is the flow stress at $T = 0$ K and

$$\beta(p,\dot{\varepsilon}) = \frac{k}{W_0(p)}\ln(\dot{\varepsilon}_0/\dot{\varepsilon}) \quad [31]$$

B. *Strain Hardening Revisited*

A number of processes may play a role in the plastic or elastic deformation of polymers: chain slippage, kinking and unkinking of chains, chain scission, cross linking, chain entanglement, and chain segment rotation. One or more of these processes will be important for a given polymer in a certain regime of temperature, strain rate, and pressure. Whatever the processes, we describe the aggregate result abstractly in terms of *units of flow*, as defined by Kauzmann:[38] "structures in a body whose motions past one another make up the unit shear stress process . . . the unit of flow may be a single molecule or a group of many molecules, and the barrier may arise directly from the repulsions between a few molecules or from some more complicated mechanism."

Here, we consider an areal density of units of flow which are somewhat analogous to dislocations in crystalline materials—line defects which are the boundaries between slipped and unslipped regions. Gilman[39] has discussed the application of dislocation theory to amorphous materials and the need to replace the constant Burgers displacement in crystalline materials with the average of a fluctuating Burgers displacement in the amorphous material.

Extending the analogy further, we assume that, at low temperatures, in the absence of thermal fluctuations, the flow stress is proportional to the square root of ρ,

$$\hat{\sigma} = \hat{\alpha}\sqrt{\rho} \quad [32]$$

where $\hat{\alpha}$ is a constant. Then, the total flow unit density may be related to the plastic strain by the differential equation described previously (Eq. [20]). But, we reinterpret the parameters in the differential equation. The term b is now the average displacement produced by a flow unit, λ is the mean free path for immobilization of flow units, and ω is the probability for mobilization of flow units. If we allow ω to have negative values, this term is to be interpreted as contributing to the immobilization of flow units in proportion to the currently existing density of immobile flow units. If b, λ, and ω are constant, the equation is easily solved and the cold flow stress becomes

$$\hat{\sigma} = B_0\sqrt{(1 - e^{-\omega\varepsilon})/\omega} \quad [33]$$

At temperatures above zero, this cold flow stress is reduced by the thermal activation factor $e^{-\alpha(p,\dot{\varepsilon})T}$.

C. *Plastic Stress-Strain Behavior of Polymers*

In order to describe the plastic stress-strain behavior of polymers, two thermally activated processes are considered, one associated with the initial yield behavior, the other associated with subsequent strain hardening. Thus, the total flow stress is written as

$$\sigma = B(p)e^{-\beta(p,\dot{\varepsilon})T} + \hat{\sigma}(\varepsilon,p)e^{-\alpha(p,\dot{\varepsilon})T} \quad [34]$$

where two terms of the form of Eq. [30] have been included. The presence of two separate deformation mechanisms was suggested in a differential scanning calorimetry study of glassy polymers by Hasan and Boyce.[40] Two distinct exotherms were found, one at temperatures below the glass transition temperature, associated with the initial yield and strain softening behavior, and the other at temperatures above the glass-transition temperature, associated with the strain hardening behavior.

D. *Total Plastic Component of Deformation*

The resulting plastic component of the deformation is described by the equation

$$\sigma = Be^{-\beta T} + B_0\sqrt{(1 - e^{-\omega\varepsilon})/\omega}\,e^{-\alpha T} \quad [35]$$

where

$$\beta = \beta_0 - \beta_1 \ln\dot{\varepsilon}$$
$$\alpha = \alpha_0 - \alpha_1 \ln\dot{\varepsilon} \quad [36]$$

and, neglecting their potential pressure dependence, β_0, β_1, α_0, are α_1 are constants. From available experimental data for polytetrafluoroethylene (PTFE), it was determined that ω depends approximately logarithmically on the strain rate and linearly on the pressure, so we choose the functional form

$$\omega = \omega_a + \omega_b \ln\dot{\varepsilon}\,\ln\dot{\varepsilon} + \omega_p p \quad [37]$$

where ω_a, ω_b, and ω_p are constants. The form of the pressure dependence for the coefficients B and B_0 follows the result of Argon,[41] who derived the expression

$$\tau = (a + cp)^{6/5} \quad [38]$$

for the low temperature shear yield stress of glassy polymers as a function of pressure. Argon's model is based on the thermally activated production of pairs of kinks in the collection of interpenetrating smooth chain molecules comprising the polymer. Thus, we choose

$$B = B_{pa}(1 + B_{pb}\, p)^{B_{pn}}$$
$$B_0 = B_{0pa}(1 + B_{0pb}\, p)^{B_{0pn}} \quad [39]$$

where B_{pa}, B_{pb}, B_{pn}, B_{0pa}, B_{0pb}, and B_{0pn} are constants.

E. *Polymer Constitutive Equation: Viscoelastic Component*

A Maxwell–Weichert model is used to describe the initial viscoelastic stress. This model is placed in series with the nonlinear dashpot described by Eq. [35], as illustrated in Figure 7. Thus, the basic equations which describe the model are

$$\sigma = \sum_{i=1}^{n} \sigma_i = \sigma_p(\varepsilon_p, \dot{\varepsilon}_p) \quad [40]$$

where $\sigma_p(\varepsilon_p, \dot{\varepsilon}_p)$ is the function in Eq. [35] relating stress to strain and strain rate,

$$\sigma_i = E_i\, \varepsilon_i^{(e)} = \eta_i\, \dot{\varepsilon}_i^{(v)} \quad [41]$$

where E_i and η_i are the modulus and viscosity of the ith component, respectively, and

$$\varepsilon = \varepsilon_i^{(e)} + \varepsilon_i^{(v)} + \varepsilon_p \quad [42]$$

where ε, $\varepsilon_i^{(e)}$,$\varepsilon_i^{(v)}$, and ε_p are the total strain, the ith-component elastic strain, the ith-component viscous strain, and the plastic strain, respectively. The viscosities, or, equivalently, the relaxation times, $\tau_i = \eta_i/E_i$, have a temperature and pressure dependence given by

$$\tau_i = \tau_{0i}\, e^{H_i/T} \quad [43]$$

where

$$H_i = H_{0i} + A_p p \quad [44]$$

F. *The Yield Stress of Polymethylmethacrylate*

The thermal activation model was applied to the yield stress of polymethylmethacrylate (PMMA) at various temperatures and strain rates,[42] as measured by Bauwens–Crowet.[43] It was shown that a volume of activation inversely proportional to the yield stress gives good agreement between the calculated and measured yield stresses.

Bauwens–Crowet's data for the compressive yield stress of PMMA divided by its shear modulus is plotted, in Figure 8, as a function of the quantity $T \ln(\dot{\varepsilon}_0/\dot{\varepsilon}) = G/\mathrm{k}$. With the correct choice of $\dot{\varepsilon}_0$, the equality holds, the quantity is the activation energy in Kelvin, and the data in the plot should coalesce into a single one-parameter curve, as they do in Figure 8 with the choice of $\dot{\varepsilon}_0 = 2 \times 10^7\ \mathrm{s}^{-1}$.

Furthermore, if the volume of activation is inversely proportional to the effective shear stress, then the curve in an ln (stress) plot should be a straight line with a slope of $-\mathrm{k}/W_0$ and intercept of $\ln(B/\mu)$. An inspection of Figure 8 shows this to be very closely the case, with $\mathrm{k}/W_0 = 2.56 \times 10^{-4}\ \mathrm{K}^{-1}$ and $B/\mu = 0.454$. These parameters then give calculated values of yield stress *vs* strain rate and temperature that match well with Bauwens–Crowet's data.

G. *Constitutive Equations for Polytetrafluoroethylene*

The model was also applied to describe the isothermal, constant strain rate stress-strain behavior of PTFE.[44,45] The parameters for use in the constitutive equation for PTFE were obtained by analyzing results reported by a number of investigators: for the plastic part, compressive split Hopkinson

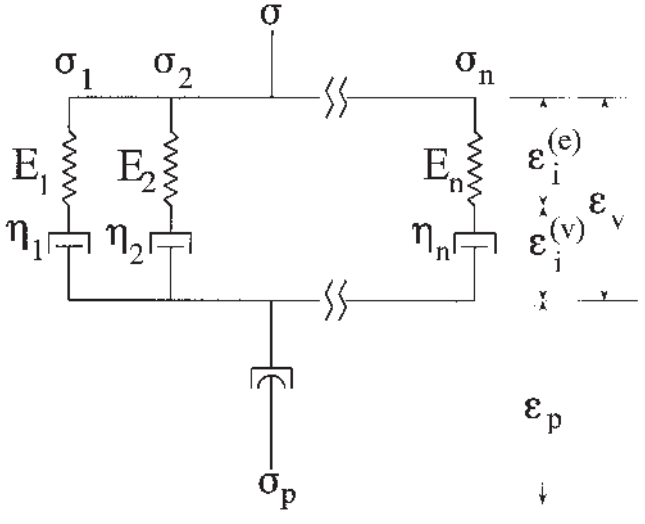

Fig. 7—Spring and dashpot diagram for Maxwell–Weichert linear viscoelasticity plus thermal activation nonlinear viscoplasticity.

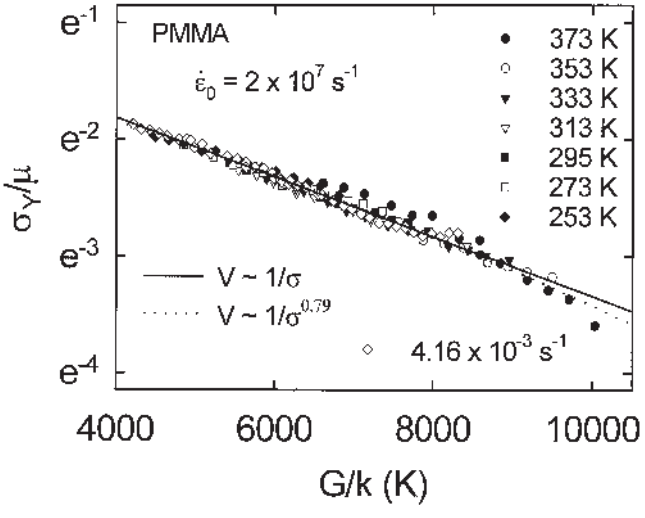

Fig. 8—Compressive yield stress divided by shear modulus *vs* $G/\mathrm{k} = T \ln(\dot{\varepsilon}_0/\dot{\varepsilon})$ for PMMA. Data of Bauwens–Crowet[43] is shown by the symbols. The solid line is the model fit for a volume of activation inversely proportional to effective shear stress, while the dotted curve is the result of a fit for a more general inverse power dependence.

pressure bar stress-strain curves at a number of strain rates as reported by Walley and Field,[46] a low temperature (130 K) Hopkinson bar stress-strain curve as reported by Walley *et al*.,[47] Hopkinson bar data at a number of temperatures and strain rates as determined by Gray *et al*.,[48] and tensile stress-strain data at various superposed hydrostatic pressures as reported by Sauer and Pae.[49] An eight component Maxwell–Weichert model was used for the viscoelastic part, with the moduli, relaxation times, and activation energies (E_i, τ_{0i}, and H_{0i}, respectively) chosen to give a reasonably good match to the shear modulus and logarithmic decrement *vs* temperature data at 1 Hz, published by McCrum.[50]

Figures 9 and 10 show stress-strain curves calculated with Eqs. [35] and [40] through [44] compared to the reported experimental data. In Figure 9, the compressive Hopkinson-bar data for stress *vs* strain at six strain rates ranging from 0.016 to 22,600 s^{-1}, reported by Walley and Field, [46] are compared to the calculated results. The change in shape of the curves with strain rate is well reproduced. The increased strain hardening with strain corresponds to negative values of ω in Eq. [35], ω becoming more negative (increased probability for immobilization of flow units) with increasing strain rate. In Figure 10, data for the tensile stress-strain with superimposed hydrostatic pressure, reported by Sauer and Pae,[49] are compared to calculated results. The change of shape of the curves with pressure is well reproduced.

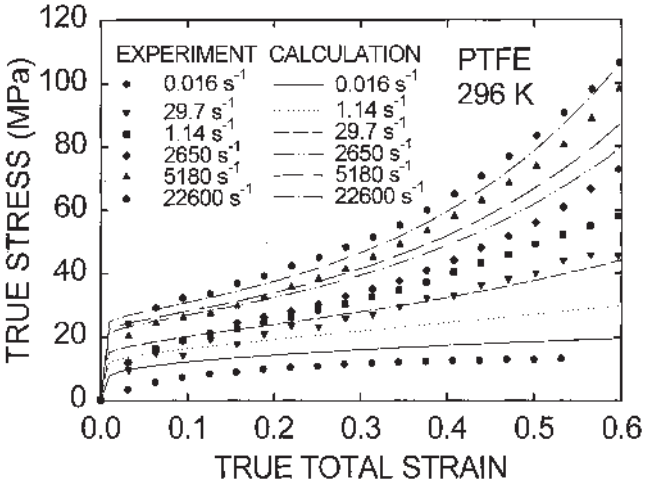

Fig. 9—Calculated compressive stress *vs* strain at several strain rates for PTFE compared with split Hopkinson pressure bar data reported by Walley and Field for PTFE.[46]

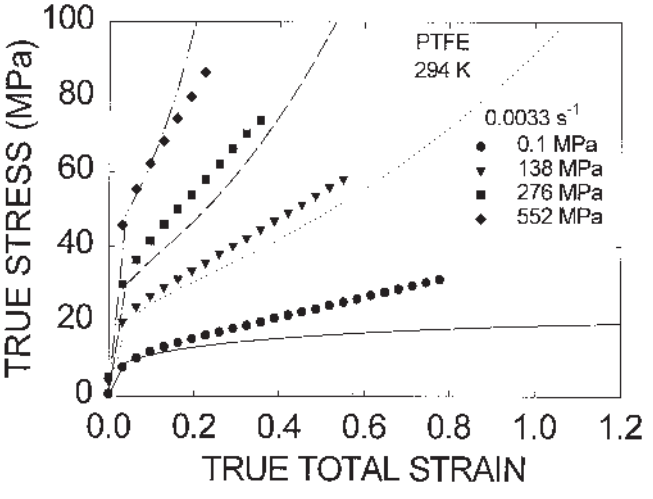

Fig. 10—Calculated compressive stress *vs* strain at several pressures for PTFE compared with tensile test data reported by Sauer and Pae.[49]

VI. CONCLUSIONS

The thermal activation model with a volume of activation inversely proportional to the effective shear stress gives an excellent description of the flow stress of a wide range of material ranging from metals to polymers. In addition, in metals, separate treatment of grain size and twinning effects leads to significant improvements in accuracy of numerical models.

ACKNOWLEDGMENTS

The work described here was supported over the years by the Office of Naval Research, by NSWC Independent Research Programs, and internally by NSWC.

REFERENCES

1. G.R. Johnson and W.H. Cook: *Proc. 7th Int. Symp. on Ballistics*, The Hague, The Netherlands, 1983, p. 541.
2. G.I. Taylor: *Proc. R. Soc. London*, 1934, vol. 145A, p. 362.
3. E. Orowan: *Z. Phys*., 1934, vol. 89, pp. 605, 614, and 634.
4. M. Polanyi: *Z. Phys*., 1934, vol. 89, p. 660.
5. H. Eyring: *J. Chem. Phys*., 1936, vol. 3, p. 107; *J. Chem. Phys*., 1936, vol. 4, p. 283.
6. P.S. Follansbee and U.F. Kocks: *Acta Metall*., 1988, vol. 36, p. 81.
7. F.J. Zerilli and R.W. Armstrong: *J. Appl. Phys*., 1987, vol. 61, p. 1816.
8. F.J. Zerilli and R.W. Armstrong: *Acta Metall. Mater*., 1992, vol. 40, pp. 1803-08.
9. U.F. Kocks, A.S. Argon, and M.F. Ashby: *Thermodynamics and Kinetics of Slip, Progress in Materials Science Vol. 19*, Pergamon, Oxford, United Kingdom, 1975.
10. C.S. Hartley: *2nd Int. Conf. on the Strength of Metals and Alloys, Vol. II,* ASM, Metals Park, OH, 1970, p. 429ff.
11. P. Feltham: *Br. J. Appl. Phys*., 1969, vol. 2, p. 377.
12. R.W. Armstrong: *(Ind.) J. Scientific Industrial Res*., 1973, vol. 32, pp. 591-598; R.W. Armstrong and J.D. Campbell: *The Microstructure and Design of Alloys*, Institute of Metals and the Iron and Steel Institute, Cambridge, United Kingdom, 1973, vol. 1, p. 529ff.
13. R.W. Armstrong and J.D. Campbell: *The Microstructure and Design of Alloys, Proc. 3rd Int. Conf. on the Strength of Metals and Alloys Vol. 1* Institute of Metals and the Iron and Steel Institute, Cambridge, United Kingdom, 1973, p. 529; H. Conrad: *J. Iron Steel Inst*., 1961, vol. 198, p. 364.
14. F.J. Zerilli and R.W. Armstrong: in *High Strain Rate Effects on Polymer, Metal and Ceramic Matrix Composites and Other Advanced Materials*, Y.D.S. Rajapakse and J.R. Vinson, eds., ASME, New York, NY, 1995, AD-Vol. 48, pp. 121-26.
15. G.R. Johnson and W.H. Cook: *Eng. Fract. Mech*., 1985, vol. 21, p. 31.
16. R.W. Armstrong and F.J. Zerilli: *J. Phys., Coll*., 1988, vol. 49 (9), p. 529.
17. R.W. Armstrong and P.J. Worthington: *Metallurgical Effects at High Strain Rates*, Plenum Press, New York, NY, 1974, p. 401.
18. W.C. Leslie: in *Metallurgical Effects at High Strain Rates*, R.W. Rohde, B.M. Butcher, J.R. Holland, and C.H. Karnes, eds., Plenum, New York, NY, 1974, p. 571.
19. F.J. Zerilli and R.W. Armstrong: *J. Appl. Phys*., 1990, vol. 68, p. 1580.
20. J.H. Bechtold and P.G. Shewmon: *Trans. ASM*, 1954, vol. 46, pp. 397-408.
21. J.H. Bechtold: *Trans. AIME*, 1956, vol. 206, pp. 142-46.
22. V. Ramachandran, R.W. Armstrong, and F.J. Zerilli: *Tungsten and Tungsten Alloys—Recent Advances*, TMS, Warrendale, PA, 1991, pp. 111-19.
23. F.J. Zerilli and R.W. Armstrong: *Shock Compression of Condensed Matter—1991*, Elsevier, Amsterdam, 1992, p. 257.

24. F.J. Zerilli and R.W. Armstrong: in *Shock Waves in Condensed Matter 1987*, Elsevier, Amsterdam, 1988, p. 273ff.
25. F.J. Zerilli and R.W. Armstrong: in *Grain Size and Mechanical Properties—Fundamentals and Applications*, M.A. Otooni, R.W. Armstrong, N.J. Grant, and K. Ishizaki, eds., Materials Research Society, Pittsburgh, PA, 1995, p. 149ff.
26. V. Ramachandran, A.T. Santhanam, and R.E. Reed-Hill: *Ind. J. Technol*., 1973, vol. 11, pp. 485-92.
27. W.H. Holt, W. Mock, F.J. Zerilli, and J.B. Clark: *Mech. Mater*., 1994, vol. 17, 195-201.
28. F.J. Zerilli and R.W. Armstrong: *Shock Compression of Condensed Matter 1989*, Elsevier, Amsterdam, 1990, p. 357ff.
29. G.I. Taylor: *Proc. R. Soc*., 1934, vol. A145, p. 362ff.
30. G.I. Taylor and H. Quinney: *Proc. R. Soc*., 1934, vol. A143, p. 307ff.
31. Y. Bergstrom: *Mater. Sci. Eng*., 1970, vol. 5, p. 193ff.
32. J. Klepaczko: *Mater. Sci. Eng*., 1975, vol. 18, pp. 121-35.
33. Y. Estrin and H. Mecking: *Acta Metall*., 1984, vol. 32, pp. 57-70.
34. D. McClean: *Mechanical Properties of Metals*, John Wiley & Sons, New York, NY, 1962.
35. S.R. Chen, G.T. Gray III, and S.R. Bingert: in *Tantalum*, E. Chen, A. Crowson, E. Lavernia, W. Ebihara, and P. Kumar, eds., TMS, Warrendale, PA, 1996, pp. 173-84.
36. F.J. Zerilli: Naval Surface Warfare Center Indian Head Division, Indian Head, MD, unpublished work, 1997.
37. B. Escaig: *Ann. Phys*., 1978, vol. 3, pp. 207-20.
38. W. Kauzmann: *Trans. Am. Inst. Min. Metall. Eng*., 1941, vol. 143, p. 57ff.
39. J.J. Gilman: *J. Appl. Phys*., 1973, vol. 44, p. 675ff.
40. O.A. Hasan and M.C. Boyce: *Polymer*, 1993, vol. 34, p. 5085ff.
41. A.S. Argon: *Phil. Mag*., 1973, vol. 28, p. 839ff.
42. F.J. Zerilli and R.W. Armstrong: in *Shock Compression of Condensed Matter—1999*, AIP Conf. Proc. 505, M.D. Furnish, L.C. Chhabildas, and R.S. Hixson, eds., American Institute of Physics, Melville, NY, 2000, pp. 531-34.
43. C. Bauwens-Crowet: *J. Mater. Sci*., 1973, vol. 8, p. 968ff; D. Fotheringham and B.W. Cherry: *J. Mater. Sci*., 1976, vol. 11, pp. 1368 and 1370.
44. F.J. Zerilli and R.W. Armstrong: *J. Phys. IV France*, 2000, vol. 10, p. 3ff.
45. F.J. Zerilli and R.W. Armstrong: in *Shock Compression of Condensed Matter—2001*, AIP Conf. Proc. 620, M.D. Furnish, N.N. Thadani, and Y. Horie, eds., American Institute of Physics, Melville, NY, 2002, pp. 657-60.
46. S.M. Walley and J.E. Field: *DYMAT J*., 1994, vol. 1, pp. 211-27 (Fig. 20).
47. S.M. Walley, J.E. Field, P.H. Pope, and N.A. Safford: *J. Phys. III France*, 1991, vol. 1, p. 1889 (Fig. 161).
48. G.T. Gray, III, C.M. Cady, and W.R. Blumenthal: *Constitutive and Damage Modeling of Inelastic Deformation and Phase Transformation, Proc. Plasticity '99*, 7th Int. Symp. on Plasticity and Its Current Applications, Akhtar S. Khan, ed., Neat Press, Fulton, MD, p. 955.
49. J.A. Sauer and K.D. Pae: *Coll. Polymer Sci*., 1974, vol. 252, p. 680ff.
50. N.G. McCrum: *J. Polymer Sci*., 1959, vol. 34, p. 355ff.